scientific reports

Check for updates

OPEN

cRGD-based MRI imaging-enhanced nanoplatform helps DOX target pancreatic cancer

Silong Li[1], Na Li[2], Qiangqiang Yin[3], Zhichen Zhang[3], Haifeng Hu[4] & Liguo Hao[3]✉

This project aims to construct cRGD functionalized mesoporous silica nanoparticles and cRGD modified mesoporous silica nanoparticles for the diagnosis and treatment of tumors, providing new ideas for targeted therapy of tumors. The mesoporous silica nanoparticles were doped with gadolinium in situ to provide excellent imaging; cRGD was coupled on the particle surface to confer particle targeting; and hyaluronic acid was loaded onto the particles by electrostatic adsorption, thereby improving the biocompatibility of the particles and prolonging their in vivo circulation time.Taking pancreatic cancer as a model, we studied its targeting ability to pancreatic cancer and its phagocytosis to cancer cells; Using methods such as cell growth experiments and flow cytometry, the anti-cancer effect and pro apoptotic effect of the system were studied. In vivo distribution, tumor targeting and therapeutic efficacy of nanoparticles evaluated in a mouse model of pancreatic cancer with loaded tumors.Evaluate the bioavailability and enrichment of nanoparticles in tumor tissue using MRI technology. Evaluate the therapeutic effect and safety through changes in tumor volume, histopathological examination, and prognosis. Characterization of the synthesis results proved that cRGD-HA-DOX-Gd_2O_3@MSN (cHDG@MSN) was successfully synthesized with a particle size of 230.83 ± 12.36 nm.In vitro drug release experiments of DOX were carried out at different pH values (5.5 and 7.4), where the release was only up to 22.65% at pH 7.4, whereas DOX release was increased up to 78.75% at pH = 5.5.The results confirm the pH responsiveness of this nanocarrier platform.The results of cytotoxicity studies showed that cHDG@MSN itself is not cytotoxic. Biosafety evaluation and hemolysis test results confirmed that the probe is highly biocompatible.Notably, Gd^{3+} significantly enhanced the T_1 contrast of the system according to MR imaging results.The apoptosis rates of SW1990 cells treated with PBS, DOX and cHDG@MSN in flow cytometry were 13.97%, 18.38% and 29.02%, respectively, demonstrating the effectiveness of the nanoprobes at the cellular level. Animal experiments demonstrated the effectiveness of nanoprobes at the pathological level and imaging level.Cells and animals demonstrated that cHDG@MSN effectively inhibited the proliferation of pancreatic cancer cells. This research further verified the pH sensitivity of the constructed compound drug delivery system to achieve accurate diagnosis and treatment of pancreatic cancer tumor cells.

Keywords Pancreatic cancer, Mesoporous silica, Magnetic resonance imaging, pH-responsive, Drug delivery

Pancreatic cancer is a fatal malignant tumor of the gastrointestinal tract and its global incidence has doubled since 25 years ago[1].and has a five-year survival rate of only 9 to 12 percent[2,3].Because pancreatic cancer is in advanced stage, its mortality rate is very high and it is difficult to carry out effective treatment.Its treatment includes surgery as well as adjuvant chemotherapy, etc.[4]. However, due to the difficulty of early diagnosis of pancreatic cancer, strong tumor aggressiveness, rapid metastasis, multi-drug resistance, etc., the effect of the currently available treatments is not satisfactory[5,6].There is an urgent need to develop new diagnostic and therapeutic methods for tumors. In recent years, with the advancement of nanotechnology, nano drug delivery systems have emerged. Compared to traditional chemotherapy, Nano-sized drug delivery system (NDDs) can effectively increase bioavailability, enhance efficacy, and reduce toxic side effects, playing a crucial role in the diagnosis and treatment of cancer[7–10].Nano drug-carrying platforms have gained wide application in more and

[1]Medical Imaging, School of Medical Technology, Qiqihar Medical University, Qiqihar, Heilongjiang Province 161006, People's Republic of China. [2]Department of Imaging Medicine and Nuclear Medicine, School of Clinical Medicine, Jiamusi University, Jiamusi 154002, People's Republic of China. [3]Department of Molecular Imaging, School of Medical Technology, Qiqihar Medical University, Qiqihar, Heilongjiang 161006, People's Republic of China. [4]Medical Imaging Center, The Second Affiliated Hospital of Qiqihar Medical University, Qiqihar, Heilongjiang 161000, People's Republic of China. ✉email: haoliguo@qmu.edu.cn

more tumor therapies as well as gene delivery, such as liposomes, which, due to their good biocompatibility[7], can enable the delivery of drugs and miRNAs in organisms and thus achieve the treatment of pancreatic cancer[8,9]. Metal nanoparticles, such as titanium, gold, manganese, and platinum nanoparticles, can be used for precision treatment of pancreatic cancer through photothermal therapy and photodynamic therapy[10,11].As a representative nano drug-carrying platform, it undoubtedly brings new hope for the precision treatment of pancreatic cancer and other tumor patients, but as a nano drug-carrying platform, there are still a series of problems such as low drug-carrying capacity, low bioavailability, low targeting ability, and poor biocompatibility. Mesoporous silica, as a potential nano-drug delivery platform, has been attracting attention for its high porosity, good biocompatibility, adjustable pore size, large specific surface area, and other advantages[12].However, the inability to target drug delivery and the shortcomings of premature drug release due to the inability of drugs to respond intelligently has limited the advancement of clinical applications.

For gating substances that are released in specific pH environments and can regulate the targeted release of drugs, the efficacy of anticancer drugs can be significantly enhanced.Hyaluronic acid, a common smart gating agent, has good biocompatibility as well as a long in vivo circulation time and can respond and target drug release in response to changes in the acidic pH environment of tumor tissues[13,14].In addition hyaluronic acid can be taken up by pancreatic cancer cells[15,16] and can promote the uptake of nano-loaded drug platforms by tumor cells through endocytosis mediated by overexpression of CD44 on the surface of pancreatic cancer cells[17].Therefore, hyaluronic acid has received extensive attention as a gating substance in the drug-targeted. Arg-Gly-Asp (RGD), the site at which integrin $\alpha v\beta_3$ recognizes its ligand, can be used to specifically recognize overexpressed $\alpha v\beta_3$ in pancreatic cancer cells by the specificity of this site[18]. Thus, the targeting of this sequence to pancreatic cancer tumors can be exploited to enhance the binding of the nano-loaded platform to cellular sites and to induce cellular uptake of the nano-loaded platform.Adriamycin, as a widely used clinical drug, has good therapeutic effects on a variety of tumors, but its application is limited by its significant myocardial toxicity[19]. In addition, MRI contrast agents commonly used in clinical practice are not only unable to target the location of tumours, but also can cause corresponding adverse reactions, such as kidney-related adverse reactions, which also limits the scope of clinical application of MRI contrast agents[20].Our probes have been improved for the inability of MRI contrast agents to target and localise tumour tissues and the difficulty of drugs to break through the tumour microenvironment, allowing the nanoprobes to have the ability to localise and aggregate tumour tissues with MRI contrast agents and to target tumours.The development of a new delivery mode for DOX that is highly water-soluble, biologically safe, highly targeted, and with few side effects is imminent.In addition to helping DOX reach the target tissue, nanocarriers reduce the side effects of chemotherapy drugs and increase their efficacy. In addition, nanocarriers effectively enhance biocompatibility and provide long-lasting stability.[21–23].

Therefore, we synthesized a new stable drug-targeting nanocarrier platform for the integration of tumor diagnosis and treatment.This nano drug-carrying platform significantly enhances the T_1 relaxation rate through gadolinium doping, and provides ready feedback on the therapeutic effect of the tumor after targeted uptake by tumor cells.The DOX in the system was taken up by tumor cells along with the nano drug-carrying platform, which reduced the drug resistance of tumor cells and the systemic adverse effects of DOX. Modification by cRGD as well as hyaluronic acid significantly enhanced the uptake as well as biocompatibility of the nano-loaded platform by tumor cells.Overall, this nano drug-carrying platform provides a new research direction for the integration of diagnosis and treatment of pancreatic cancer.

Materials and methods

Materials

All reagents listed below are analytical grade and do not require one-step purification.Cetyltrimethylammonium bromide (CTAB), tetraethyl orthosilicate (TEOS), N-hydroxysuccinimide (NHS), and N-ethyl-N'-(3-dimethylaminopropyl) carbodiimide (EDC) were purchased from Aladdin (Shanghai, China); hyaluronic acid (HA), adriamycin was purchased from Shanghai McLean Biochemical Co.The cell lines used in this study were obtained from Starfish Bioscience Ltd.They are ethically procured and used.High Resolution Transmission Electron Microscope (FEI Talos F200S), ASAP-2460 Automated Surface Area and Porosity Analyzer, Shimadzu UV-2450 Spectrophotometer, Hitachi 7000 Fluorescence Spectrophotometer, RF-5301PC Fourier Transform Infrared Spectrophotometer.

Synthesis of cRGD-HA-DOX-Gd_2O_3@MSN

Synthesis of gadolinium-doped mesoporous silica particles (Gd_2O_3@MSN)

Add 0.5 g of CTAB, 1 ml of sodium hydroxide solution (140 mg/ml) and 220 ml of DI water to a 500 ml egg shaped bottle.When magnetic stirring was employed, the temperature was elevated to 80 °C and the reaction proceeded for 30 min. Subsequently, 2 mL of TEOS solution was introduced into the reaction system in a gradual manner, and the reaction was permitted to continue for 2 h. The reaction was conducted in a single step.Subsequently, 20 mL of a $GdCl_3.6H_2O$ solution was added slowly, and the reaction was continued for one hour. Then, 0.5 mL of a TEOS solution was added slowly and uniformly, and the reaction lasted for two hours. Once the reaction was complete, the solution was collected and allowed to stand for 12 h.The Gd_2O_3@MSN samples were collected by centrifugation and subsequently washed with deionised water and anhydrous ethanol on five occasions.The collection process was conducted for a period of 10 min. Thereafter, the cleaned samples were placed in a drying oven at a temperature of 60 degrees Celsius for a period of 24 h. The samples were then subjected to a further drying period at 60 degrees Celsius for a period of 10 min.Following drying, the samples were removed and ground, and then calcined in a muffle furnace at 550 °C for 6 h to eliminate residual CTAB. The resulting product was gadolinium oxide-modified mesoporous silica, designated Gd_2O_3@MSN.

Synthesis of DOX-Gd_2O_3@MSN
Take 0.5 g of Gd_2O_3@MSN, slowly add 10 mL of 10 mg/mL DOX solution dropwise and dissolve it by ultrasonication, stirring in a beaker (300 r/min) and let it react away from light for 12 h, then use high speed centrifugation (9000 r/min, 15 min) to remove free DOX, and the obtained product was washed by centrifugation with deionised water for four times and then lyophilised, which was obtained as DOX-Gd_2O_3@MSN.

Synthesis of HA-DOX-Gd_2O_3@MSN
50 mg of DOX-Gd_2O_3@MSN was taken and dissolved in viscous HA solution (5 mg/mL, 5 mL) and stirred overnight at room temperature. After centrifugation (10000 r/min, 10 min), the resulting product was washed with water three times to obtain HA-DOX-Gd_2O_3@MSN.

cRGD-HA-DOX-Gd_2O_3@MSN synthesized
50 mg of HA-DOX-Gd_2O_3@MSN was taken and dispersed together with N-(3-dimethylaminopropyl-N-ethylcarbodiimide) hydrochloride (EDC, 10 mg) and N-hydroxysuccinimide (NHS, 10 mg) in 15 mL of buffer with pH 6.0 at room temperature with stirring (400 r/min), and the reaction lasted for 1 h. After the reaction was continued for 1 h, 5 mg of cRGD was added to it. After the reaction lasted for 1 h, 5 mg of cRGD was added to it to continue the reaction for 18 h. The reaction product was dialyzed in a dialysis bag for 24 h to remove the cRGD, as well as EDC and NHS, and cRGD-HA-DOX-Gd_2O_3@MSN was obtained by centrifugation.

Characterization measurement
The morphology and structure of the material were finely characterized using transmission electron microscopy (TEM, FEI TalosF200x, USA), and its composition was analyzed. The characteristic absorption peaks of the nanoparticle were studied using a Fourier transform infrared spectrophotometer (6800 JASCO, Marseille, France). The particle size, PDI, and zeta potential were measured using a laser particle size analyzer. The imaging characteristics of nanoparticles in vivo were confirmed using a 3.0 T nuclear magnetic resonance spectrometer.

Stability and drug release from nanocarrier platforms
To assess the stability of cHDG@MSN, we prepared a 1 mg/mL solution of cHDG@MSN as well as a 1 mg/mL solution of Gd_2O_3@MSN for polymer dispersibility index determination (n = 3).To study the release efficiency of DOX in different pH environments, we added 5 mL (1 mg/mL) of cHDG@MSN to two dialysis bags, adjusted the solution pH to 5.5 and 7.4, and agitated the solution at 400 rpm.At 0, 4, 8, 12, 16, 20, and 24 h, we removed 3 mL of the solution and measured its absorbance at 233 nm.In order to maintain the volume of the original solution, we added 3 mL of fresh PBS at the same time during each sampling procedure. drug loading and encapsulation rates were calculated using the following equations.

$$DLC\,(\%) = \frac{\text{weight of the drug in NPs}}{\text{weight of NPs}} \times 100\%$$

$$EE\ (\%) = \frac{\text{weight of the drug in NPs}}{\text{weight of the drug in feed}} \times 100\%$$

T_1 relaxation rate and in vitro magnetic resonance imaging

Inductively coupled plasma mass spectrometry (ICP-MS, Agilent 720 ES, USA), and ICP-MS were used to detect the presence of free Gd3 + in the synthesised probes, which were placed in phosphate-buffered saline in an environment of pH 5.5 for 48 h. Next, we assessed the T_1 relaxation of the probes at different concentrations of.

Biocompatibility and biotoxicity

The stability of the probes was evaluated by monitoring the alteration in particle size of the nanocarrier platforms in deionised water over a seven-day period. In brief, the probes were dissolved in deionised water, and the hydrated particle size was measured and documented at 1, 3, 5, and 7 days. The findings were presented as follows.

Prior to analysis, samples were dissolved in different aqueous media (deionised water, phosphate buffered salts and 10% foetal bovine serum) at a concentration of 1 mg/mL. The cHDG@MSN Gd^{3+} content was determined by ICPOES (Mason, OH, USA).

The biological toxicity of the sample was analysed using CCK-8, H&E staining, a haemolysis test and a blood test. In brief, cells were inoculated into 96-well plates at a density of 6×10^3 cells per well and then cultured in RPMI 1640 containing 1% penicillin and 10% foetal bovine serum for 24 h at 37 °C and 5% CO_2 to allow for the cells to adhere to the surface of the well.Subsequently, varying concentrations of probe clusters (5, 10, 20, 50, 100 and 200 μg/mL) were introduced to the medium. Following a 24-h incubation period, a CCK-8 solution (10 μL) was added to the wells of a 96-well plate and further incubated for a further two hours. The sample was then incubated for a further two hours with the CCK-8 solution. Finally, the absorbance of each well was measured at 490 nm using a tablet reader (SAFIRE2, TECAN, Mennedorf, Switzerland). The cell viability was calculated using the following formula:

$$cellviability(\%) = \frac{OD_{Sample} - OD_{blank}}{OD_{Control} - OD_{blank}} \times 100\%$$

Haemocompatibility was assessed by first centrifuging the erythrocytes at 2500 r/min for 6 min at 4 °C. The erythrocytes were then washed and purified repeatedly with saline.Then, 2 mL of probe (10, 20, 40, 80, or 160 μg/

mL) was dissolved with 2 mL of diluted RBC suspension (4% v/v) in saline.The system was then incubated at 37 °C for 4 h before being concentrated at 8000 r/min for 10 min.Measure the absorbance of the supernatant at 576 nmusing a UV visible spectrophotometer..The formula for the rate of haemolysis was as follows.

$$\text{Hemolysis}\,(\%) = \frac{A_{\text{Sample}} - A_{\text{Negative Control}}}{A_{\text{Positive Control}} - A_{\text{Negative Control}}} \times 100\%$$

The in vivo toxicity of the nanocarrier platform was tested in female nude mice (18–20 g).The Animal Ethics Committee of Qiqihar Medical University (No. QMU-AECC-2022–120) analysed all studies.Nude mice were injected with saline and probe via the tail vein. 7 days later, the nude mice were put to death and the major organs (heart, liver, spleen, lungs and kidneys) were removed for pathological examination.

Cellular uptake of probes in vitro

Use laser confocal microscopy to observe its absorption of cells.SW1990 cells were provided by the Molecular Imaging Laboratory of Qiqihar Medical University.Cells were injected into confocal dishes and cultured for 24 h until the logarithmic growth phase was reached.After cell adhesion, 50 μg/mL of the nano-loading platform was added for incubation. Then, the cells were rinsed with PBS to remove excess probe that was not taken up by the cells.The washed cells were fixed with 4% paraformaldehyde for 20 min and then treated with DAPI for 10 min. cellular uptake of the probe was observed using confocal microscopy.

In vitro anti-tumour effects of probes

The in vitro therapeutic effects of the carried nanoclusters were evaluated. Free DOX (concentrations of 0.05, 0.1, 0.2, 0.5, and 1 μg/mL), DG@MSN, and cHDG@MSN (concentrations of 1, 2, 4, 10, and 20 μg/mL, respectively) were incubated with Panc-1 and SW1990 cells for 24 h, and cell survival was determined by CCK-8 colourimetric assay.The experimental methods and data processing methods were the same as those used in the cytotoxicity assay.A 6-well plate was first filled with pancreatic cancer cells at a density of 2×10^5/mL to assess the effect of cHDG@MSN on apoptosis.After 12 h of incubation, cHDG@MSN, DG@MSN and PBS (blank group) were added to each well and incubated continuously for 48 h. In this study, flow cytometry was used to detect apoptosis.

In vivo anti-tumour effects of probes

Female nude rats weighing between 15 and 18 g were purchased from Qiqihar Medical University. Upon arrival, the rats were divided into 4 groups and housed under standardised conditions of temperature (23 ± 2 °C), humidity (55 ± 1%) and 12/12 h light/dark cycle. Animals were allowed to acclimatise for one week before the start of the experiment.

All methods were performed in accordance with the relevant guidelines and regulations of the ARRIVE guidelines and reviewed and authorised by the Ethics Committee for the Care and Use of Laboratory Animals of Qiqihar Medical University [ID: QMU-AECC-2021–174].

Nude mice with tumours were randomly assigned to four groups (n = 4) and given a tail vein injection of 100 μL of PBS, DOX, DG@MSN or cHDG@MSN (2 mg/kg).The first dose was given on the first day of the experiment and then every other day for a total of 15 d.The length and width of the tumours were measured with vernier calipers every other day from day one. The tumours were subsequently excised and all nude mice were executed after the treatment cycle.The tumour tissue was then sectioned, paraffin embedded and preserved in 4% paraformaldehyde solution. Tumour staining and TUNEL were performed using H&E and light microscopy. We used the formula shown below to calculate the volume of the tumour.

$$\mathbf{V} = \frac{1}{2}\mathbf{a}\mathbf{b}^2$$

In vivo imaging

By in vivo magnetic resonance imaging, 100 μL of the probe was injected into hormonal nude mice via the tail vein. Images were acquired with a 3.0 T MRI scanner at 0, 30 min, 60 min, and 180 min after injection, respectively.

Statistical methods

Statistical analysis was performed using SPSS 22.0 software, and the measurement results were represented by ($\overline{x} \pm s$); The count data was subjected to t-test, and $P < 0.05$ was considered significant.

Results and discussion

Synthesis and characterisation

Integration of diagnosis and treatment can be achieved through the nano drug-carrying platform.In this project, targeted nanocarriers for imaging and drug delivery were successfully synthesised.The synthesis of mesoporous silica systems mounted with cRGD has been described in the above method (see Fig. 1).Firstly, MSN particles doped with gadolinium ions were prepared. Subsequently, the free DOX was loaded inside the Gd_2O_3@MSN for the purpose of drug loading.Next, hyaluronic acid was modified onto DOX-loaded Gd_2O_3@MSN by stirring method through electrostatic adsorption. Figure 2A high-resolution transmission electron microscopy image showed that the average diameter of Gd_2O_3@MSN reached (205.83 ± 7.95) nm, displaying a clearly defined pore structure and regular morphological features. Figure 2B Scanning electron microscopy showed uniform distribution of hyaluronic acid, demonstrating that HA was encapsulated on the surface of hyaluronic acid.EDS

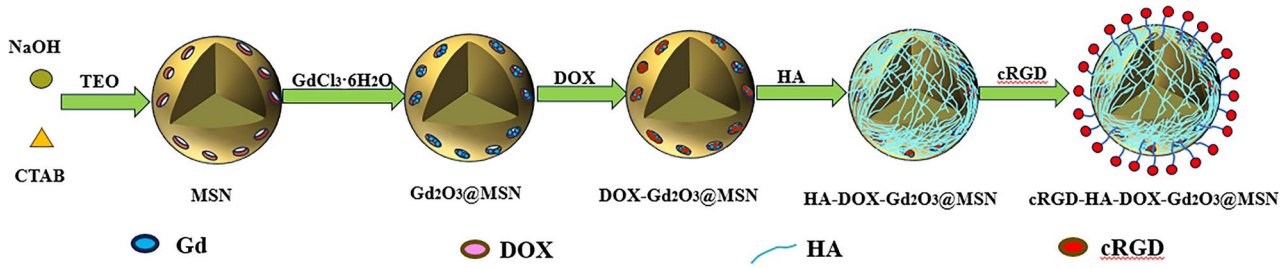

Fig. 1. Synthesis of cRGD-HA-Gd_2O_3@MSN.

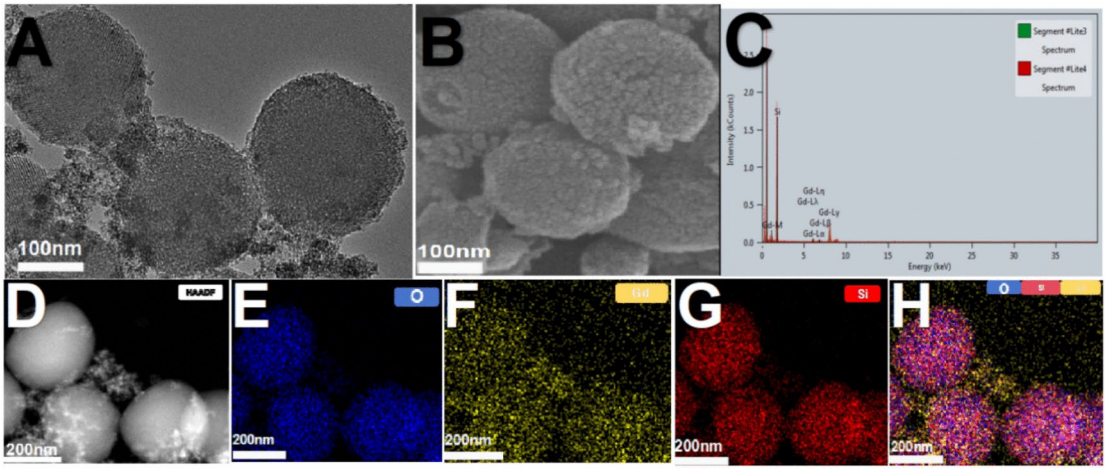

Fig. 2. Electron microscopy imaging of cHDG@MSN, (A)TEM image of Gd_2O_3@MSN (**B**) SEM imaging of HDG@MSN (**C**) EDS spectrum of Gd_2O_3@MSN (**D**–**H**) HAADF-STEM image and elemental mapping of Gd_2O_3@MSN.

mapping images (Fig. 2C) showed the content of Gd, Si and O in Gd_2O_3@MSN.The exact gadolinium content was determined to be 6.46% by ICP-MS (Agilent 720 ES, Shanghai, China) analysis results. The above results significantly indicate that the element Gd has been successfully loaded into the mesoporous silica.The elemental mapping (Fig. 2D-H) by high-angle annular dark-field scanning provides further visual evidence of the core–shell structure and elemental distribution in Gd_2O_3@MSN.

All the drug-carrying nanoplatforms were successfully synthesised using the above method in Fig. 3A. The zeta potential of cHDG@MSN shown in Fig. 3D changed considerably from -37.2 mV to 27.7 mV, which indicates the successful modification of cRGD as well as HA on the Gd_2O_3@MSN surface.After HA encapsulation, the surface charge of the HDG@MSN changed significantly to -11.63 mV.This could explain the presence of a large number of carboxyl groups in HA. However, the zeta potential of CHDG@MSN again increased dramatically, which could be due to the consumption of many negative carboxyl groups during the cRGD coupling process[24]. The hydrated particle sizes of Gd_2O_3@MSN, DG@MSN, HDG@MSN, and cHDG@MSN were subsequently obtained in ddH_2O (Fig. 3E), which increased as the surface of Gd_2O_3@MSN continued to change, with hydrated particle sizes of 207 nm, 209.5 nm,233.5 nm, and 240.3 nm, respectively (Fig. 3E).The polydispersity index (PDI) of cHDG@MSN (0.30) was slightly lower than that of Gd_2O_3@MSN (0.33), suggesting that the HA coating may moderately improve the dispersion stability of cHDG@MSN (Fig. 3F).In addition, the particle sizes measured by dynamic light scattering were larger than those measured by transmission electron microscopy. This is most likely due to the hydrated layer and the small amount of aggregation caused by the nanoparticles in the aqueous environment.The IR spectrum of MSN, shown in Fig. 3B, produced a characteristic peak at 1080 cm-1 corresponding to the Si–O-Si vibration, confirming the synthesis of mesoporous silica.And we also found the absorption peak at 1635 cm^{-1} , which indicates the C-N scaling vibration and variable angular vibration of the amine group in cRGD, which suggests that the target molecule, cRGD, was successfully modified with an absorption peak.

The pore size and specific surface area of MSNs with different modifications were studied at 77 K.The NPs curves were analyzed using the Bruno-Emmett-Taylor method.The Gd_2O_3@MSN exhibits a specific surface area of 888.55m^2/g and a pore volume of 1.25 cm^3/g, indicating its outstanding drug loading performance.For DG@MSN, the above parameters were reduced to 423.57 m^2/g and 0.85 cm^3/g, respectively, suggesting that DOX may have been successfully loaded onto Gd_2O_3@MSN.For HDG@MSN, the above parameters decreased to 252.50

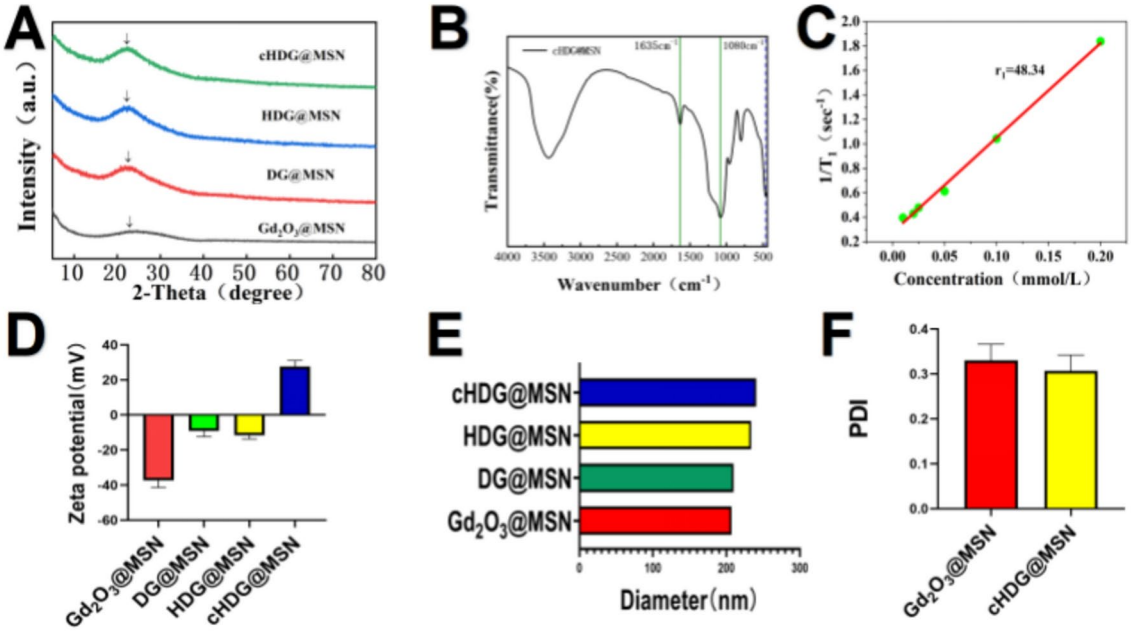

Fig. 3. Structural characterization of drug-carrying nanoplatforms, (**A**)XRD detection of Gd_2O_3 (**B**) FTIR spectra of cHDG@MSN (**C**) T_1 relaxation rate of Gd_2O_3@MSN at 0.5 T (**D**) Zeta potential values of different mono-dispersed silica (n = 3) (**E**) Particle sizes of the four nano-loaded platforms (**F**) PDI values of Gd_2O_3@MSN and cHDG@MSN.

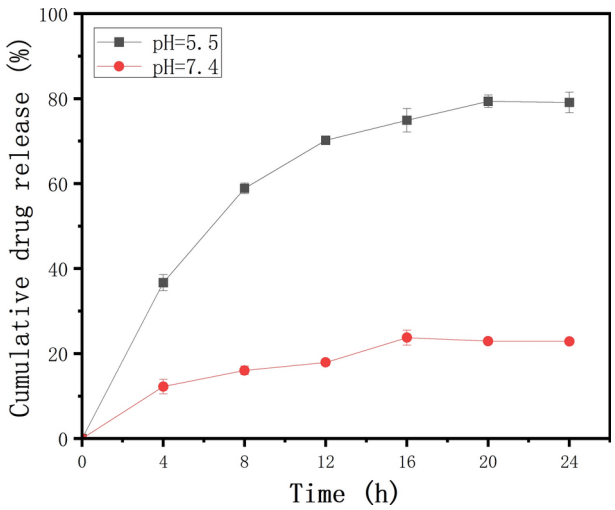

Fig. 4. Drug release profile of cHDG@MSN.

m^2/g and 0.50 cm^3/g, respectively, indicating that HA covered the Gd_2O_3@MSN surface[25].The results are shown in Table 1.

Assessment of T_1 relaxivity

The findings of this study substantiate that cHDG@MSN induces the release of DOX in response to pH fluctuations. Subsequently, the prospective utilisation of cHDG@MSN as an MRI contrast agent was investigated utilising a 0.5 T NMI20 Ananyst NMR system.The relaxation rate (r_1) of Gd_2O_3@MSN was 48.34 mM^{-1} s^{-1} ($R^2 = 0.997$) (Fig. 3C), which was significantly higher than that of clinically applied Gd-DTPA, indicating that Gd_2O_3@MSN has the potential to be used as an MRI contrast agent and can be used to target tumor tissues with precision imaging[26].

	Surface area (m^2 /g)	Pore volume (cm^3 /g)	Pore size (nm)
Gd_2O_3@MSN	888.55	1.25	5.29
DG@MSN	423.17	0.85	3.87
HDG@MSN	416.57	0.50	3.20

Table 1. Parameters of N_2 adsorption and desorption by different stages of nanocarrier platforms.

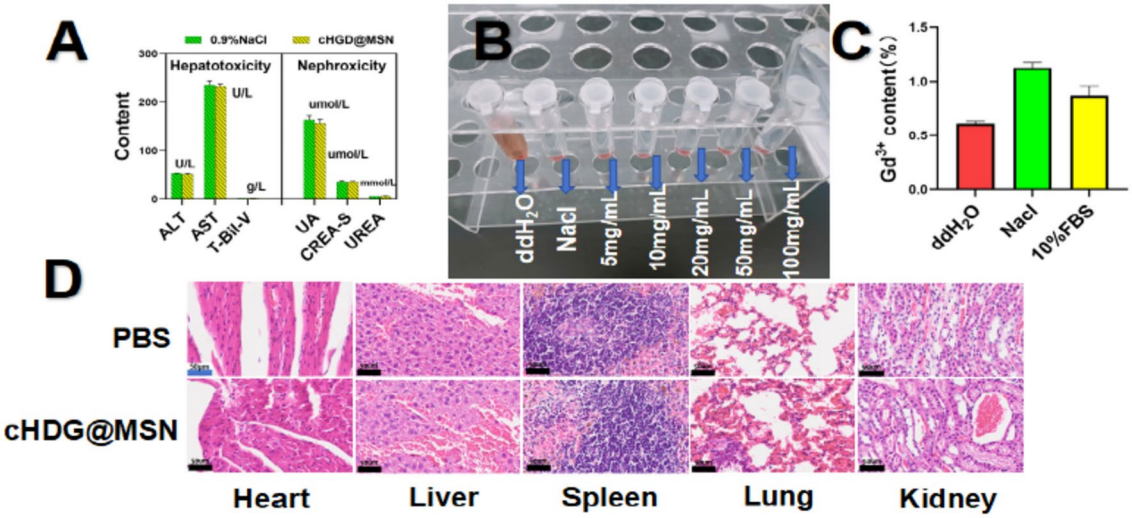

Fig. 5. (**A**) Biochemical indices of liver and kidney function (n = 5, ns: p > 0.05) (**B**) Hemolysis assay of cHDG@MSN (**C**) Leakage rate of gadolinium ions in three solution environments, (**D**) H&E staining images of anatomical organs of nude mice treated with PBS and cHDG@MSN.

Loading and release behavior of drugs

Since the microenvironment in which tumor cells live is acidic. Therefore, cHDG@MSN is released when the pH is acidic, which helps to kill tumor cells more effectively.The drug loading of DOX was calculated using the intensity of the UV–visible adsorption peak of DOX at 233 nm and the standard curve, which was 9.27%, and the calculated encapsulation rate was 46.35%.In this study, we investigated the release behavior of cHDG@MSN under different pH conditions, and in order to simulate the in vivo environment, we performed incubation experiments of the probes at 37 ℃.Two different pH values, 7.4 and 5.5, were set in this experiment as a way to simulate the pH of normal blood and tumor microenvironment.After 24 h of incubation, the release reached 22.65% at neutral pH (7.4), while DOX release increased to 78.75% at pH 5.5 (Fig. 4).This successfully demonstrated drug release from cHDG@MSN via pH changes.This pH-dependent release reduces the release of DOX from neutral environments, such as the blood, prolongs the circulation time of the drug in the bloodstream, and promotes the release of DOX at the tumor site, thereby reducing side effects on other tissues and decreasing the myocardial toxicity of DOX[27] (Fig. 5, 6).

Biocompatibility and biotoxicity

A prerequisite for the application of probes to living organisms is that they must have good compatibility, colloidal stability and low biotoxicity.In this study, the colloidal stability of cHDG@MSN was investigated by determining the changes in the hydrated particle size of cHDG@MSN in deionized water.The hydrated particle size of cHDG@MSN in deionized water did not change significantly, indicating that cHDG@MSN has good colloidal stability.As shown in Fig. 7D, the survival rates of SW1990 and H6C7 cells were more than 80% even after treatment with 200 mg/mL of Gd_2O_3@MSN, indicating that the nanocarrier platforms have low cytotoxicity. The hemocompatibility of cHDG@MSN was then assessed by hemolysis. As shown in Fig. 4B, the hemolysis rate was below 5% at all concentrations, which satisfied the biosafety requirements.

Healthy Balb/c mice were injected with cHDG@MSN solution (5 mg/kg) or 0.9% NaCl solution, respectively. The above animals were then observed for 7 days to assess the in vivo biotoxicity of cHDG@MSN.Body weights of nude mice in both saline and cHDG@MSN groups grew normally.In addition, blood tests showed that mice injected with cHDG@MSN did not exhibit any significant signs of liver or kidney impairment (Fig. 5A).

In addition, the release of free Gd^{3+} from cHDG@MSN is an important factor to consider, and high concentrations of Gd^{3+} in the body may lead to kidney damage[28].We measured the leakage of Gd^{3+} by ICP-OES analysis. The results showed that the release of Gd^{3+} was less than 2% in all cases. (Fig. 5C).

According to the results of H&E staining experiments, cHDG@MSN-treated major organs, such as the heart, liver, spleen, lungs, and kidneys, did not show any pathologic changes (Fig. 5D).These findings suggest that cHDG@MSN has good biocompatibility.

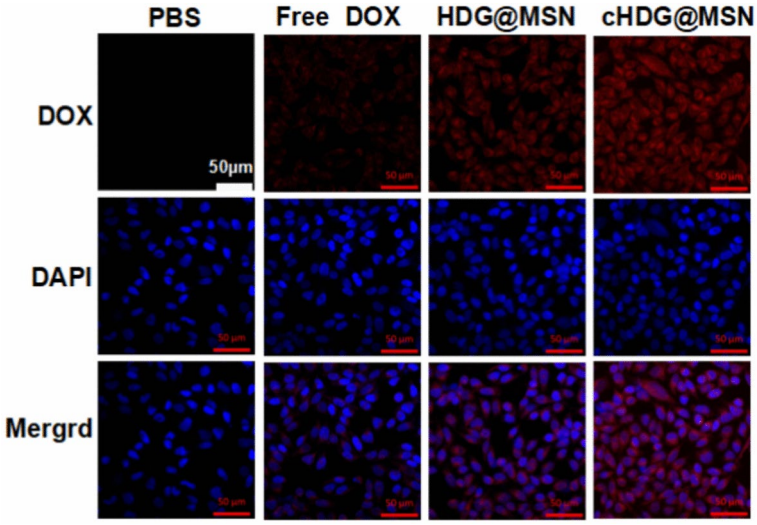

Fig. 6. Confocal laser scanning microscopy images of SW1990 cells after incubation with PBS, Free Dox, HDG@MSN and cHDG@MSN. Red and blue colors represent DOX and DAPI fluorescence, respectively (scale bar: 50 μm).

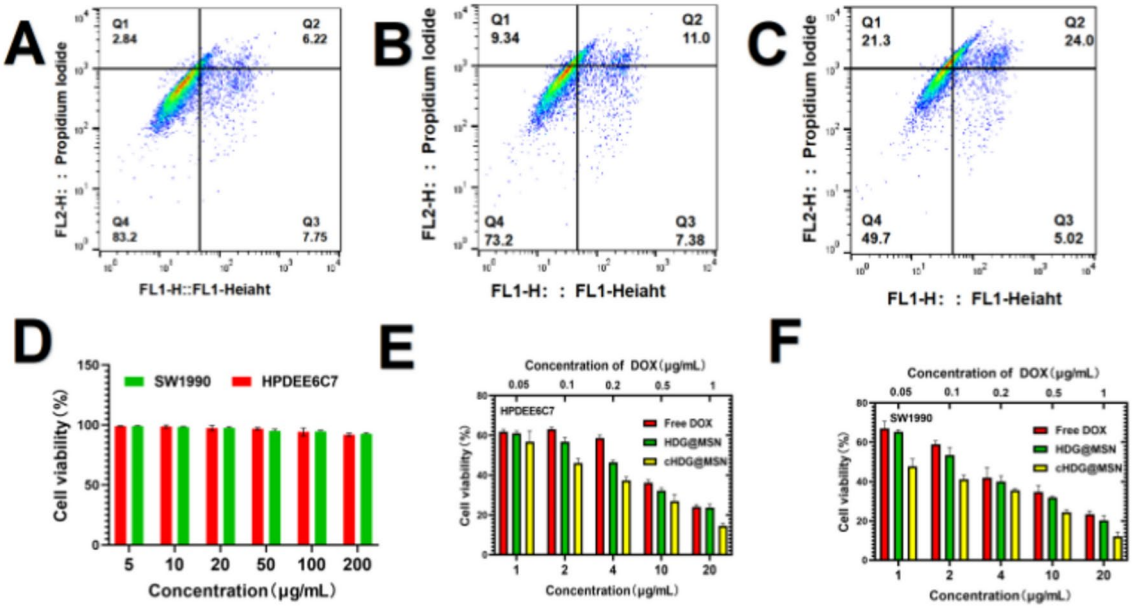

Fig. 7. (**A**–**C**) Relative viability of SW1990 cell survival A: Free DOX B: HDG@MSN C: cHDG@MSN (**D**) Viability of SW1990 and HPDE6C7 cells after 24 h of Gd_2O_3@MSN treatment. (**E**,**F**) Relative cell viability after incubation with free DOX, HDG@MSN and cHDG@MSN at different DOX concentrations.E: HPDEEC7.

In vitro cellular uptake of drug-carrying nanoplatforms

Tumor imaging and therapy relies on effective cellular uptake of nano-loaded drug platforms.Therefore, we investigated the cellular uptake of DOX and cHDG@MSN.In this study, cellular uptake of the probe was directly observed using confocal laser scanning microscopy (CLSM) with DOX and cHDG@MSN co-scanning microscopy.As shown in the figure, strong red fluorescence was observed in the DOX-treated SW1990 cells, indicating that DOX could effectively enter the cancer cells.Compared to DOX, cHDG@MSN-treated cells exhibited more intense red fluorescence, indicating better cellular uptake of cHDG@MSN (Fig. 6).The integrated optical density of each group of cells was then obtained and analyzed using Image-Pro Plus and GraphPad Prism 9.5.0.The results also showed that the signal intensity in the targeted group was significantly higher than that in the non-targeted group, due to the fact that the integrin $\alpha v\beta_3$ can be particularly highly expressed in SW1990 cells, and the cyclic RGD peptide can preferentially bind this integrin.

In vitro anti-tumor effects of nano-loaded drug platforms.

Safety and non-toxicity are prerequisites for the application of the delivery system. As shown in Fig. 7D, the survival rate of SW1990 cells and HPDE6C7 cells was more than 85% when the Gd_2O_3@MSN concentration reached 200 μg/mL.

The intracellular cHDG@MSN releases DOX, which then prevents cell division, stalling the cell in G2/M phase and leading to cancer cell death. The therapeutic effect of cHDG@MSN was assessed using SW1990 and H6C7 cells. It is noteworthy that the mortality of H6C7 and SW1990 cells increased significantly in all groups with increasing concentrations.It is of greater significance that, at the same dose of DOX, the mortality rate in the cHDG@MSN group was markedly higher than that in the non-targeted DOX group. This indicates that cHDG@MSN has a superior capacity to inhibit tumour proliferation and destroy pancreatic cancer cells in a targeted manner. Subsequent apoptosis experiments were conducted, and the resulting flow cytometry data are presented in Figs. 7A-C.The apoptosis rates of SW1990 cells treated with PBS, DOX and cHDG@MSN were 13.97%, 18.38% and 29.02%, respectively. It was observed that the apoptosis rate was higher in H6C7 cells treated with cHDG@MSN compared to DOX. As shown in Fig. 7E-F, the killing ability of the drugs on HPDE6C7 and SW1990 cells was enhanced with the increase of DOX concentration. Among them, the cell death rate in the cHDG@MSN group was higher than that in theHDG@MSN group. This indicated that cRGD amplified the antitumour effect of the chemotherapeutic drug DOX. In addition, at the same concentration, the mortality rate of SW1990 cells was similar to that of HPDE6C7 cells, but interestingly, the cell mortality rate of SW1990 was superior. This suggests that the successful attachment of the targeting substance cRGD to the nanoparticles can enhance the targeting of the nanoparticles and effectively promote the apoptosis of pancreatic cancer cells, thus enhancing their anti-tumour effects.This suggests that the combination of the targeted portion of cRGD with the nanoclusters enhanced the targeting of the nanoclusters and effectively increased apoptosis of pancreatic cancer cells, thereby enhancing the other therapeutic effects of DOX[29].

In vivo anti-tumor effects of nano-loaded drug platforms

The remarkable efficacy of cHDG@MSN in vitro inspired us to further explore its anti-tumor ability in vivo. Figure 8A shows the overall animal test design route.Considering the desirable therapeutic effect and significant cytotoxicity observed in vitro, the nude mice in the DG@NPs group did not show any death associated with the administration of the drug throughout the treatment experiments, and the changes in body weight were within the normal fluctuation range (Fig. 8B), which did not show any statistically significant difference compared with the control group.Fifteen days after tail vein injection of cHDG@MSN at a dose of 2 mg/kg, the experimental animals were euthanized and the tumor volume of the cancerous mice was recorded.As shown in Fig. 7C, cHDG@MSN significantly suppressed tumor volume compared with the PBS group (Fig. 8E). The targeted ligands accelerated the accumulation of cHDG@MSN at the tumor site, which enhanced its antitumor activity, and this is the reason why cHDG@MSN exhibited the most potent tumor inhibitory effect.The final tumor weight is shown in Fig. 8D.And the echocardiographic results of the tumor-bearing nude mice showed no obvious abnormalities in their cardiac function, which proved that the nano drug-carrying platform could reduce the myocardial toxicity of DOX (Fig. 9B).

At the end of the treatment, a portion of the tumor tissue was cut into sections and then stained with H&E staining and TUNEL assay for further analysis.As shown in Fig. 8A, nude mice treated with cHDG@MSN had the fewest cancer cells and a higher percentage of apoptosis and necrosis than the other treatment groups.All of

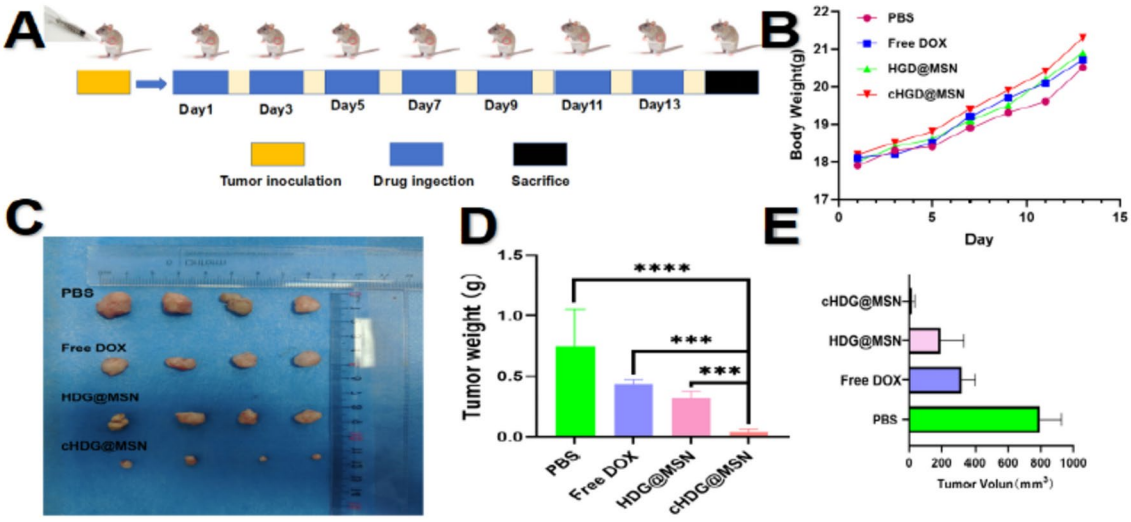

Fig. 8. (**A**) Experimental design of the efficacy of cHDG@MSN in treating subcutaneous tumor model of pancreatic cancer, (**B**) Changes in body weight of nude mice in each group. (**C**) Graph of the effect of tumor treatment after treatment, (**D**) Final mean tumor weight after 15 days of treatment, (**E**) Changes in tumor volume.

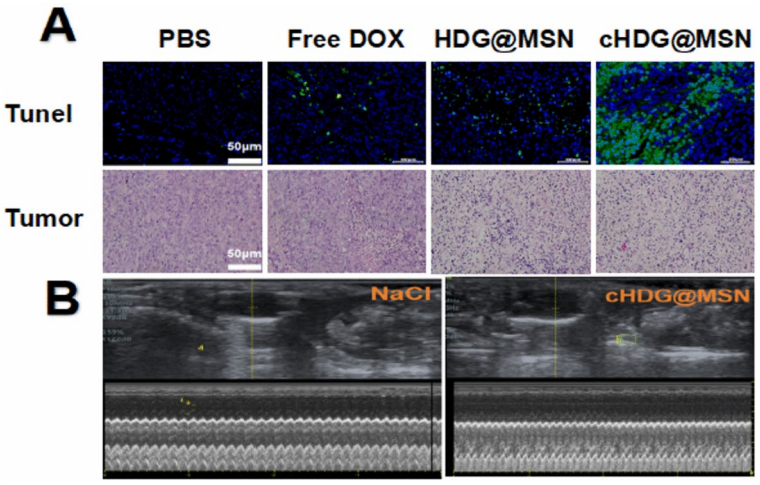

Fig. 9. (**A**) HE-stained tumor sections and TUNEL images of each group of tumor tissues, (**B**) Echocardiography of tumor-bearing nude mice.

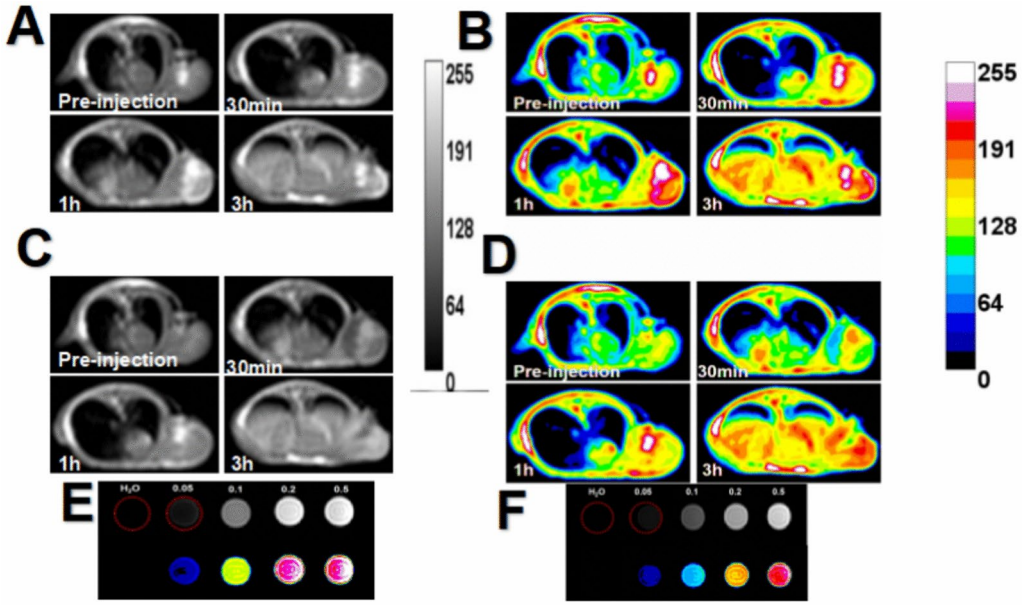

Fig. 10. In vivo T_1 imaging of nano-loaded drug platforms. (**A**) Changes in T_1 signal intensity at cHDG@MSN tumor site injection, (**B**) Pseudo-color image of injected cHDG@MSN tumor site, (**C**) Changes in T_1 signal intensity at the site of injected HDG@MSN tumors, (**D**), (**E**) In vitro changes with different concentrations of cHDG@MSN and its signal intensity, (**F**) In vitro with different concentrations of gadopentetate dextran and changes in signal intensity.

the above results suggest that the binding of cRGD can help these nanoclusters target tumors more effectively and produce more potent anti-tumor effects.

Ex vivo and in vivo imaging

A 3.0 T MRI scanner was employed to assess the in vitro and in vivo MRI capabilities of cHDG@MSN. Nude mice were administered 5 mg/kg of HDG@MSN and cHDG@MSN 5 mg, and T_1-weighted images were acquired at designated time points.As illustrated in Fig. 10A, the T_1WIs of the tumour tissues exhibited a gradual enhancement following the administration of cHDG@MSN. In comparison to the T_1WI of the nude mouse tumours injected with HDG@MSN (Fig. 10C), the T_1WI of the tumours injected with cHDG@MSN exhibited a markedly brighter signal, which may be attributed to the enhanced targeting ability of the nanoclusters. These findings suggest that the systemic administration of cHDG@MSN facilitates the early detection of tumours and enables precise treatment. A comparison of the efficacy of different concentrations of cHDG@MSN and gadopentetate dextran in vitro, as demonstrated in Fig. 10E, indicates that cHDG@MSN is comparable to

clinically adopted enhancers. In light of the aforementioned evidence, it can be concluded that cHDG@MSN represents a promising candidate for use in accurate and effective cancer therapies. Figures 10B, D, and F are pseudo-colour images intended to show the effect.

Conclusion

In this study, we developed a cHDG@MSN for magnetic resonance bimodal and targeted drug delivery. the results of colloidal stability, haemolysis assay and toxicity assay showed that cHDG@MSN has good stability and biocompatibility. Both hyaluronic acid and cRGD significantly promoted the uptake of the probe by tumour cells. In vitro cellular uptake assay showed that cHDG@MSN has a good targeting effect on pancreatic cancer cells. In addition, cHDG@MSN significantly enhances the contrast effect of magnetic resonance imaging (MRI), which can be used to monitor tumour development. Therefore, the nanocarrier platform investigated in this work can be used for T_1-mode MRI and tumour-targeted delivery of DOX as a novel nanomaterial for the integration of tumour diagnosis and treatment. However, our cell- and animal-based investigations are not sufficiently representative of medical applications, and further in-depth studies are needed to properly evaluate the efficacy of the probes.

Data availability

The datasets used and/or analysed during the current study available from the corresponding author on reasonable request.

Received: 11 November 2024; Accepted: 21 February 2025
Published online: 28 February 2025

References

1. Klein, A. P. 2021 Pancreatic cancer epidemiology: understanding the role of lifestyle and inherited risk factors. *Nat. Rev. Gastroenterol. Hepatol.* **18**(7), 493–502. https://doi.org/10.1038/s41575-021-00457-x (2021).
2. Siegel, R. L., Miller, K. D., Wagle, N. S. & Jemal, A. Cancer statistics, 2023. *CA Cancer J Clin.* **73**(1), 17–48. https://doi.org/10.3322/caac.21763 (2023).
3. Miller, K. D. et al. Cancer treatment and survivorship statistics, 2022. *CA Cancer J. Clin.* **72**(5), 409–436. https://doi.org/10.3322/caac.21731 (2022).
4. Park, W., Chawla, A. & O'Reilly, E. M. Pancreatic Cancer: A Review. *JAMA* **326**(9), 851–862 (2021).
5. Wood, L. D., Canto, M. I., Jaffee, E. M. & Simeone, D. M. Pancreatic Cancer: Pathogenesis, Screening, Diagnosis, and Treatment. *Gastroenterology* https://doi.org/10.1053/j.gastro.2022.03.056 (2022).
6. Hosein, A. N., Brekken, R. A. & Maitra, A. Pancreatic cancer stroma: an update on therapeutic targeting strategies. *Nat. Rev. Gastroenterol. Hepatol.* https://doi.org/10.1038/s41575-020-0300-1 (2020).
7. Dymek, M. & Sikora, E. Liposomes as biocompatible and smart delivery systems - the current state. *Adv. Colloid Interface Sci.* https://doi.org/10.1016/j.cis.2022.102757 (2022).
8. Wang-Gillam A, Li CP, Bodoky G, Dean A, Shan YS, Jameson G, Macarulla T, Lee KH, Cunningham D, Blanc JF, Hubner RA, Chiu CF, Schwartsmann G, Siveke JT, Braiteh F, Moyo V, Belanger B, Dhindsa N, Bayever E, Von Hoff DD, Chen LT; NAPOLI-1 Study Group. Nanoliposomal irinotecan with fluorouracil and folinic acid in metastatic pancreatic cancer after previous gemcitabine-based therapy (NAPOLI-1): a global, randomised, open-label, phase 3 trial. Lancet. https://doi.org/10.1016/S0140-6736(15)00986-1. (2016).
9. Obaid G, Bano S, Thomsen H, Callaghan S, Shah N, Swain JWR, Jin W, Ding X, Cameron CG, McFarland SA, Wu J, Vangel M, Stoilova-McPhie S, Zhao J, Mino-Kenudson M, Lin C, Hasan T. Remediating Desmoplasia with EGFR-Targeted Photoactivable Multi-Inhibitor Liposomes Doubles Overall Survival in Pancreatic Cancer. Adv Sci (Weinh), https://doi.org/10.1002/advs.202104594. (2022).
10. Xie, Z. et al. Biocompatible Two-Dimensional Titanium Nanosheets for Multimodal Imaging-Guided Cancer Theranostics. *ACS Appl Mater Interfaces.* **11**(25), 22129–22140. https://doi.org/10.1021/acsami.9b04628 (2019).
11. Shi, Y. et al. Fe-Doped Polyoxometalate as Acid-Aggregated Nanoplatform for NIR-II Photothermal-Enhanced Chemodynamic Therapy. *Adv. Healthc. Mater.* https://doi.org/10.1002/adhm.202000005 (2020).
12. Tang, F., Li, L. & Chen, D. Mesoporous silica nanoparticles: synthesis, biocompatibility and drug delivery. *Adv. Mater.* **24**(12), 1504–1534. https://doi.org/10.1002/adma.201104763 (2012).
13. Yan, S. et al. "One Stone, Four Birds" Ion Engineering to Fabricate Versatile Core-Shell Organosilica Nanoparticles for Intelligent Nanotheranostics. *ACS Nano.* **16**(6), 9785–9798. https://doi.org/10.1021/acsnano.2c03550 (2022).
14. Kang, X. et al. Dual-Cascade Responsive Nanoparticles Enhance Pancreatic Cancer Therapy by Eliminating Tumor-Resident Intracellular Bacteria. *Adv. Mater.* https://doi.org/10.1002/adma.202206765 (2022).
15. Kim, P. K. et al. Hyaluronic acid fuels pancreatic cancer cell growth. *Elife* **24**, 62645. https://doi.org/10.7554/eLife.62645.PMID:34951587;PMCID:PMC8730721 (2021).
16. Sato, N., Kohi, S., Hirata, K. & Goggins, M. 2016 Role of hyaluronan in pancreatic cancer biology and therapy: Once again in the spotlight. *Cancer Sci.* **107**(5), 569–575. https://doi.org/10.1111/cas.12913 (2016).
17. Kesharwani, P., Chadar, R., Sheikh, A., Rizg, W. Y. & Safhi, A. Y. CD44-Targeted Nanocarrier for Cancer Therapy. *Front. Pharmacol.* https://doi.org/10.3389/fphar.2021.800481 (2022).
18. Nieberler, M. et al. Exploring the Role of RGD-Recognizing Integrins in Cancer. *Cancers (Basel)* **9**(9), 116 (2017).
19. Minotti, G., Menna, P., Salvatorelli, E., Cairo, G. & Gianni, L. Anthracyclines: molecular advances and pharmacologic developments in antitumor activity and cardiotoxicity. *Pharmacol Rev.* **56**(2), 185–229. https://doi.org/10.1124/pr.56.2.6 (2004).
20. Sam, A. D. 2nd. et al. Safety of gadolinium contrast angiography in patients with chronic renal insufficiency. *J. Vasc. Surg.* **38**(2), 313–318. https://doi.org/10.1016/s0741-5214(03)00315-x (2003).
21. Kapse-Mistry, S., Govender, T., Srivastava, R. & Yergeri, M. Nanodrug delivery in reversing multidrug resistance in cancer cells. *Front Pharmacol.* https://doi.org/10.3389/fphar.2014.00159 (2014).
22. Shapira, A., Livney, Y. D., Broxterman, H. J. & Assaraf, Y. G. Nanomedicine for targeted cancer therapy: towards the overcoming of drug resistance. *Drug Resist Updat.* **14**(3), 150–163. https://doi.org/10.1016/j.drup.2011.01.003 (2011).
23. Lee, H. et al. Mannosylated acrylic acid)-coated mesoporous silica nanoparticles for anticancer therapy. *J. Control Release.* https://doi.org/10.1016/j.jconrel.2022.06.064 (2022).
24. Hu, L. L. H., Li, Z. Y., Zhuo, R. X. & Zhang, X. Z. MMP-responsive theranostic nanoplatform based on mesoporous silica nanoparticles for tumor imaging and targeted drug delivery. *J. Mater Chem. B* https://doi.org/10.1039/c5tb02490k (2016).

25. Yu, M. et al. Hyaluronic acid modified mesoporous silica nanoparticles for targeted drug delivery to CD44-overexpressing cancer cells. *Nanoscale* **5**(1), 178–183. https://doi.org/10.1039/c2nr32145a (2013).
26. Li, Z., Guo, J., Qi, G., Zhang, M. & Hao, L. pH-Responsive Drug Delivery and Imaging Study of Hybrid Mesoporous Silica Nanoparticles. *Molecules* **27**(19), 6519 (2022).
27. Qi, G. et al. A Novel pH-Responsive Iron Oxide Core-Shell Magnetic Mesoporous Silica Nanoparticle (M-MSN) System Encapsulating Doxorubicin (DOX) and Glucose Oxidase (Gox) for Pancreatic Cancer Treatment. *Int. J. Nanomed.* https://doi.org/10.2147/IJN.S436253 (2023).
28. Mehran, R., Dangas, G. D. & Weisbord, S. D. Contrast-Associated Acute Kidney Injury. *N. Engl. J. Med.* **380**(22), 2146–2155. https://doi.org/10.1056/NEJMra1805256 (2019).
29. Wang, S. et al. cRGD-Conjugated GdIO Nanoclusters for the Theranostics of Pancreatic Cancer through the Combination of T1–T2 Dual-Modal MRI and DTX Delivery. *Molecules* **28**(16), 6134 (2023).

Author contributions
NL and LH supervised and analysed all experiments.SL L designed and conducted the study, analysed the data and wrote the manuscript. Manuscript.SL L, NL and ZC Z HF H completed in vivo experiments. All authors assisted with data/image analysis and completed in vitro experiments. All authors have read and agreed to the published version of the manuscript.

Funding
This study was supported by grants from Heilongjiang Province Student Innovation and Entrepreneurship Training Programme Project (202311230033).

Declarations

Competing interests
The authors declare no competing interests.

Ethics approval
Implement according to the experimental procedures formulated by the Animal Ethics Research Center of Qiqihar Medical University*(QMU-AECC-2021–174). This study followed the ARRIVE guidelines and was conducted in accordance with the "Regulations on the Management of Experimental Animals of the People's Republic of China" and relevant regulations.Used in animal experiments. Our research approach pays sufficient attention to the living conditions of experimental animals and minimizes the results of the experiments.

Additional information
Correspondence and requests for materials should be addressed to L.H.